Microscopic calculations for normal and polarized liquid ^{3}He

E. Manousakis, S. Fantoni,* V. R. Pandharipande, and Q. N. Usmani†
Department of Physics and Materials Research Laboratory, University of Illinois at Urbana—Champaign, Urbana, Illinois 61801
(Received 16 May 1983)

Accurate variational calculations are carried out for the ground-state quantities of the normal and fully spin-polarized phases of liquid ^{3}He. The variational wave functions include semioptimized two-body, three-body, and backflow correlations. Expectation values are calculated using Fermi-hypernetted-chain summation techniques. The elementary diagrams are summed with the scaling approximation developed earlier for Bose liquids. Results of calculations using the interatomic potential of Aziz *et al.* from equilibrium to melting density are reported. The calculated equation of state, sound velocity, and liquid structure function for the normal phase are in close agreement with the experimental data. The three-body and backflow correlations are found to be important in achieving this agreement with experiment. The energy of the spin-polarized phase is found to be above that of the normal phase over the entire liquid density range, and it is found that the backflow correlations are necessary to achieve this result.

I. INTRODUCTION

The ground state of liquid ^{3}He has been extensively studied in the past decade. Starting from a microscopic interaction between helium atoms one attempts to explain the known zero-temperature equation of state and liquid structure function. In addition, the microscopic theory should show that the energy of the spin-polarized liquid is above that of the normal liquid in the density region over which the liquid exists. The methods developed in this paper and the calculations presented achieve these goals.

Basically two approaches have been adopted to calculate the ground-state properties of liquid ^{3}He. These are the variational and the Green's-function Monte Carlo (GFMC) approaches. The variational calculations use either MC (Refs. 1—3) or the integral-equation methods[4] to calculate binding energies. Recent variational calculations[4,1] have shown that the Jastrow-Slater wave function, containing only pair correlations depending upon distances r_{ij} is not adequate. The two-body backflow and three-body correlation have a large effect on the binding energy.

The ground state of Bose liquid ^{4}He can be calculated almost exactly with the GFMC method.[6,7] The results obtained with the HFDHE2 interatomic potential of Aziz *et al.*[8] are in very close agreement with the experimental energies of the liquid and solid ^{4}He over the density range $\rho=(0.36-0.6)\sigma^{-3}$, where $\sigma=2.556$ Å is the Lennard-Jones unit of length in helium liquids. The density of liquid ^{3}He has the range $\rho=(0.277-0.4)\sigma^{-3}$, and we expect the Aziz potential to provide a good microscopic Hamiltonian. In all the calculations reported in this work this potential has been used.

There are practical problems associated with the application of GFMC technique to the ground state of Fermi liquids.[4] Owing to these the only available result is an upper bound of approximately -2.2 K to the binding energy at equilibrium density against an experimental value of -2.47 K. The best variational MC energy[1] obtained thus far with wave functions containing three-body and backflow correlations is ~ 1.9 K; moreover, variational wave functions that do not include the two-body backflow correlation give a lower energy for the spin-polarized liquid than for the normal liquid.[3] Attempts have been made to improve upon the variational results by using correlated basis perturbation theory[9] and it has been suggested[10] that a spin $(\vec{\sigma}_i\cdot\vec{\sigma}_j)$ correlation may be responsible for bringing the energy of the normal state below that of the spin-polarized state.

In two preceding papers[11,12] on Bose liquid ^{4}He we developed an accurate integral-equation method based on the hypernetted-chain technique and the scaling approximation for elementary diagrams (HNC/S), and used semioptimized pair correlation $f_2(r_{ij})$ and a more general three-body correlation than that used in MC calculations.[1,13] The results obtained in these calculations are within 3% of experiment and the GFMC results. The same correlation functions were used more recently to study the energies of droplets of liquid ^{4}He containing up to 728 atoms by the variational MC method.[14] The results of these MC calculations are within $\sim 4\%$ of the presumably exact GFMC energies, and they confirm the HNC/S results.

In the present work we develop the FHNC/S method, which generalizes HNC/S to Fermi liquids, and use it to study the ground-state properties of liquid ^{3}He. Semioptimized $f_2(r_{ij})$ is used, and the "box terms" in the Monte Carlo[1,13] three-body $f_3(\vec{r}_{ij},\vec{r}_{ik})$ and backflow $f_k(r_{ij})$ correlations are removed. The variational energies decrease to approximately -2.35 K at equilibrium density, and the calculated equation of state $E(\rho)$ and structure function $S(k)$ are in close agreement with experiment. The energy of the spin-polarized liquid is above that of the normal over the liquid density range, and it is found that the backflow correlations are important to achieve this result.

Section II deals with the Jastrow-Slater calculations with the FHNC/S method, the three-body and backflow correlations are treated in Secs. III and IV. These sections

also give results obtained with wave functions for which MC results are available, to test the accuracy of the FHNC/S method.

II. FHNC/S METHOD

The Jastrow-Slater variational wave function of a Fermi liquid is defined as

$$\Psi=\prod_{\substack{i,j\\ i<j}} f_2(r_{ij})\Phi \ , \tag{2.1}$$

where Φ is the Fermi-gas wave function and $f_2(r_{ij})$ is a two-body correlation function. The two-body distribution function $g(r_{ij})$ is obtained from the FHNC equations[15] as

$$g(r_{ij})=g_{dd}(r_{ij})+2g_{de}(r_{ij})+g_{ee}(r_{ij}) \ . \tag{2.2}$$

The $g_{xy}(r_{ij})$ give contributions to g, and $xy=dd$, de, and ee denote terms in which neither i nor j is exchanged, j is exchanged, and both i and j are exchanged, respectively. The g_{xy} are given by

$$g_{dd}(r_{ij})=f_2^2(r_{ij})\exp[N_{dd}(r_{ij})+E_{dd}(r_{ij})] \ , \tag{2.3a}$$

$$g_{de}(r_{ij})=g_{dd}(r_{ij})[N_{de}(r_{ij})+E_{de}(r_{ij})] \ , \tag{2.3b}$$

$$g_{ee}(r_{ij})=g_{dd}(r_{ij}) \times\left[-\frac{1}{\nu}L^2(r_{ij})+N_{ee}(r_{ij})+E_{ee}(r_{ij}) +[N_{de}(r_{ij})+E_{de}(r_{ij})]^2\right] , \tag{2.3c}$$

$$L(r_{ij})=-l(k_Fr_{ij})+\nu[N_{cc}(r_{ij})+E_{cc}(r_{ij})] \ . \tag{2.4}$$

Here ν is the spin degeneracy, k_F is the Fermi momentum, and $l(k_Fr)$ is the familiar Slater function

$$l(x)=3j_1(x)/x \ . \tag{2.5}$$

N_{xy} denote sums of nodal diagrams, E_{xy} denote sums of elementary diagrams, and the composite diagrams are generated by Eqs. (2.3). The functions N_{cc} and E_{cc} denote sums of diagrams in which i and j are exchanged in an incomplete exchange loop. It is convenient to define a distribution function $g_{cc}(r_{ij})$,

$$g_{cc}(r_{ij})=g_{dd}(r_{ij})L(r_{ij})/\nu \ , \tag{2.6}$$

whose contribution is contained in the first term of $g_{ee}(r_{ij})$.

The sums of nodal diagrams are obtained from the following integral equations:

$$N_{dd}(r_{ij})=\Gamma((g_{dd}+g_{de}-N_{dd}-N_{de}-1)_{ik},(g_{dd}-1)_{kj})+\Gamma((g_{dd}-N_{dd}-1)_{ik},(g_{de})_{kj}) \ , \tag{2.7a}$$

$$N_{de}(r_{ij})=\Gamma((g_{dd}+g_{de}-N_{dd}-N_{de}-1)_{ik},(g_{de})_{kj})+\Gamma((g_{dd}-N_{dd}-1)_{ik},(g_{ee})_{kj}) \ , \tag{2.7b}$$

$$N_{ee}(r_{ij})=\Gamma((g_{de}+g_{ee}-N_{de}-N_{ee})_{ik},(g_{de})_{kj})+\Gamma((g_{ed}-N_{ed})_{ik},(g_{ee})_{kj}) \ , \tag{2.7c}$$

$$N_{cc}(r_{ij})=\Gamma((g_{cc}-N_{cc}+l/\nu)_{ik},(g_{cc})_{kj}) \ , \tag{2.7d}$$

where Γ is the convolution integral defined as

$$\Gamma(x_{ik},y_{kj})\equiv\rho\int d^3r_k\,x(r_{ik})y(r_{kj}) \tag{2.8}$$

and ρ is the density of atoms.

There is no analytic method available to evaluate the sum E_{xy} of the elementary diagrams. In the FHNC approximation E_{xy} are set to zero, while in the FHNC/4 approximation[16] they are evaluated from four-point diagrams with generalized bonds. Some of these are shown in Fig. 1. The dashed lines in these diagrams represent a $g_{dd}-1$ bond, while a half-dashed, half-solid line represents a g_{de} bond and a solid line denotes g_{ee}. Thus the direct and exchange ends of bonds are, respectively, denoted by dashed and solid lines. We cannot have diagrams in which the exchange ends of two bonds touch at a point. The g_{cc} bonds are denoted by lines with arrows depicting the direction of exchange loops. The g_{cc} bonds must form closed loops, or contribute to E_{cc}. The solid points represent the coordinates of internal points, and we have to integrate over them. Open circles represent $\vec{r}_i$ and $\vec{r}_j$, or external points in general. The contribution of diagram (1.4) of Fig. 1 to $E_{de,4}$ is, for example,

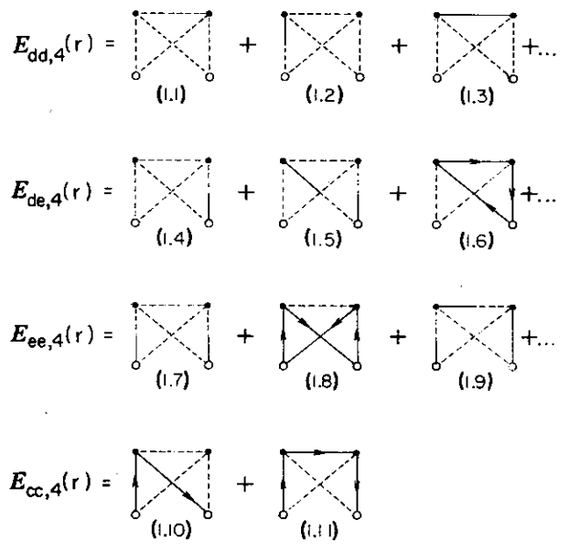

FIG. 1. Some E_4 elementary diagrams. Black dots and open circles represent internal and external points. Various bonds are explained in the text.

$$E_{de,4}(1.4)=\rho^2\int (g_{dd}-1)_{ik}(g_{dd}-1)_{il}(g_{dd}-1)_{kl} \times(g_{dd}-1)_{jk}(g_{ed})_{jl}d^3r_k d^3r_l \ . \quad (2.9)$$

The three-particle distribution function can be expressed as

$$g_3(r_{ij},r_{jk},r_{ki})=\sum_{\text{exch}} g_{xy}(r_{ij})g_{y'z}(r_{jk})g_{z'x'}(r_{ki}) \times[1+A_{x''y''z''}(r_{ij},r_{jk},r_{ki})] \ , \quad (2.10)$$

where $A_{x''y''z''}$ is the sum of Abe contributions[17] with exchange patterns denoted by x'', y'', and z'' at the vertices i, j, and k. The sum over exchanges in (2.10) is over all allowed combinations of $x,y,z,x',\ldots,z''$ which form correct exchange patterns. In the FHNC approximation the Abe contribution is neglected; the g_3 is then a sum of 31 terms.[4] In the FHNC/4 approximation[16] A is approximated with $A_{xyz,4}$ the contribution of four-point Abe diagrams. Some of these are shown in Fig. 2, and for example, the contribution of diagram (2.2) is

$$A_{ddd,4}(2.2)=\rho\int (g_{dd}-1)_{il}(g_{dd}-1)_{jl}(g_{ed})_{kl}d^3r_l \ . \quad (2.11)$$

The energy of the liquid can be calculated in different ways by integrating the kinetic-energy terms by parts.[18] The three commonly used forms[16] are E_{JF} (Jackson-Feenberg), E_{CW} (Clark-Westhaus), and E_{PB} (Pandharipande-Bethe). The E_{PB} is obtained from $\nabla^2(\prod f_2)\Phi$, and is given by

$$E_{\text{PB}}=T_F+W+U+W_F+U_F \ , \quad (2.12)$$

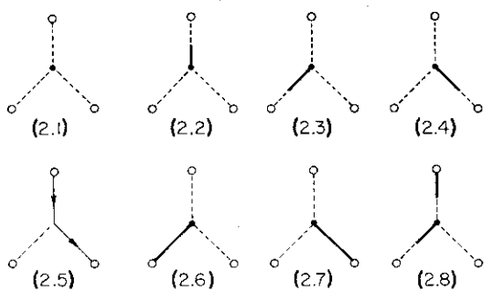

FIG. 2. Some A_4 diagrams in the Abe expansion of the three-body distribution function.

where T_F is the Fermi-gas kinetic energy (i.e., $\nabla^2\Phi$ term)

$$T_F=\frac{3}{5}\frac{\hbar^2}{2m}k_F^2 \ , \quad (2.13)$$

W and U contain contributions from the interaction and the ∇^2 operating on the f_2's

$$W=\frac{\rho}{2}\int d^3r\, g(r)\left[v(r)-\frac{\hbar^2}{m}\frac{\nabla^2 f_2}{f_2}\right] , \quad (2.14)$$

$$U=-\frac{\hbar^2}{2m}\rho^2\int d^3r_{12}d^3r_{13}g_3(r_{12},r_{23},r_{31}) \times\frac{\vec{\nabla}_1 f_2(r_{12})\cdot\vec{\nabla}_1 f_2(r_{13})}{f_2(r_{12})f_2(r_{13})} \ , \quad (2.15)$$

and W_F and U_F give contributions from $\vec{\nabla}f_2\cdot\vec{\nabla}\Phi$ terms,

$$W_F=-\frac{\hbar^2}{2m}\rho\int d^3r\, g_{cc}(r)\frac{1}{f_2}f_2' l' \ , \quad (2.16)$$

$$U_F=-\frac{\hbar^2}{2m}\rho^2\int d^3r_{12}d^3r_{13}\frac{1}{f_2(r_{12})}f_2'(r_{12})l'_{13}\hat{r}_{12}\cdot\hat{r}_{13} \times\{g_{cc}(r_{13})g_{dy}(r_{12})[g_{dy'}(r_{32})-1+g_{dy'}(r_{32})A_{ddd}]+g_{dd}(r_{13})g_{cc}(r_{23})g_{cc}(r_{31})(1+A_{ddd})\} \ , \quad (2.17)$$

where the f_2' and l' denote $\partial f_2/\partial r$ and $\partial l/\partial r$. A sum of y and y' is implied, and, for sake of brevity, only A_{ddd} terms are included in Eq. (2.17).

The E_{CW} is obtained from $[\vec{\nabla}(\prod f_2)\Phi]^2$,

$$E_{\text{CW}}=T_F+W_{\text{CW}}-U \ , \quad (2.18)$$

$$W_{\text{CW}}=\tfrac{1}{2}\rho\int d^3r\, g(r)\left[v(r)+\frac{\hbar^2}{m}\frac{(f_2')^2}{f_2^2}\right] , \quad (2.19)$$

and the E_{JF} is obtained from a combination of $\nabla^2(\prod f_2)\Phi^*$, $[\nabla(\prod f_2)\Phi]^2$, and the $\nabla^2(\prod f_2)\Phi$. It is given by

$$E_{\text{JF}}=T_F+W_B+W_\phi+U_\phi \ . \quad (2.20)$$

The form of W_B is identical to the energy of the Bose liquid

$$W_B=\tfrac{1}{2}\rho\int d^3r\, g(r)\left[v(r)-\frac{\hbar^2}{2m}\frac{\nabla^2 f_2-(f_2')^2}{f_2}\right] , \quad (2.21)$$

$$W_\phi=-\frac{\hbar^2}{4m}\frac{\rho}{\nu}\int d^3r\,((g_{dd}-1)\{[l-\nu(N_{cc}+E_{cc})]\nabla^2 l+(l')^2\}-\nu g_{dd}E_{cc}\nabla^2 l) \ , \quad (2.22)$$

$$U_\phi = -\frac{\hbar^2}{4m}\frac{\rho}{2}\int d^3r_{12}d^3r_{13}[(g_{dd}-1)l']_{12}[(g_{dd}-1)l']_{13}g_{cc}(r_{23})\hat{r}_{12}\cdot\hat{r}_{13}+\cdots , \tag{2.23}$$

where the ellipsis includes the Abe contribution. The three-body term U in the $E_{\rm PB}$ and $E_{\rm CW}$ is large (~ 1 K at equilibrium ρ_0), while the U_ϕ in $E_{\rm JF}$ is very small (~ 0.004 K at ρ_0). Thus $E_{\rm PB}$ and $E_{\rm CW}$ are sensitive to the $g_3(r_{ij},r_{jk},r_{ki})$ while $E_{\rm JF}$ is not. However, $E_{\rm JF}$ and $E_{\rm CW}$ are very sensitive to the two-body $g(r)$, while a cancellation between $-\nabla^2 f_2$ and vf_2 makes $E_{\rm PB}$ less sensitive to errors in $g(r)$.

If we sum over all elementary diagrams these three expressions will give the same expectation value. However, at the FHNC or FHNC/4 level of approximation they give different energies as illustrated in Fig. 3 and Ref. 16. The distribution functions (calculated with the FHNC/S equations are shown in Fig. 4. We note that g_{de} and g_{ee} are quite small, and so the elementary and Abe diagrams should be dominated by the $g_{dd}-1$ bond. The diagrams formed with $g_{dd}-1$ should approximately satisfy the scaling properties discussed in Ref. 9.

In the present work we calculate the elementary diagrams (1.1) of Fig. 1 and (2.1) of Fig. 2 with the bond $g(r)-1$. In this way all four-point diagrams linear in g_{de} and g_{ee} are counted correctly. Let E_4 and A_4 be the contributions of these diagrams. The scaling approximation is then taken to be

$$E_{dd}(r)=(1+s)E_4 , \tag{2.24a}$$

$$E_{xy}(r)=0 \quad \text{for } xy\neq dd \tag{2.24b}$$

$$A_{ddd}(r_{ij},r_{jk},r_{ki})=(1+s/2)A_4(r_{ij},r_{jk},r_{ki}) , \tag{2.25a}$$

$$A_{xyz}=0 \quad \text{for } x,y,z\neq d,d,d . \tag{2.25b}$$

The energies $E_{\rm PB}$, $E_{\rm JF}$, and $E_{\rm CW}$ are calculated as a function of the scaling variable s, which is determined from the condition

$$E_{\rm PB}(s)=E_{\rm JF}(s)\equiv E(\text{FHNC/S}) . \tag{2.26}$$

The $E_{\rm PB}$ increases, while $E_{\rm JF}$ and $E_{\rm CW}$ decrease as s increases. In normal liquid ^{3}He the $E_{\rm CW}(s)$ is very close to the E(FHNC/S), but in the spin-polarized liquid $E_{\rm CW}(s)$ is a little above the E(FHNC/S) as illustrated in Fig. 5.

Results of calculations with the pair correlation

$$f_2(r)=\exp[-\tfrac{1}{2}(b/r)^5] \tag{2.27}$$

are shown in Tables I and II and Figs. 3 and 5. The FHNC/S energies are in close agreement with the available MC results. The success of this FHNC/S method may be partly due to the fact that g_{de} and g_{ee} tend to cancel each other (Fig. 2), and hence there are substantial cancellations between elementary and Abe diagrams with g_{de} and g_{ee} bonds. Thus our approximation of diagrams having two or more g_{de},g_{ee} bonds may not be too relevant. In addition, the scaling equations (2.24) and (2.25) will correct for the neglect of exchange elementary and Abe diagrams.

The problem of calculating the optimum $f_2(r)$ for the

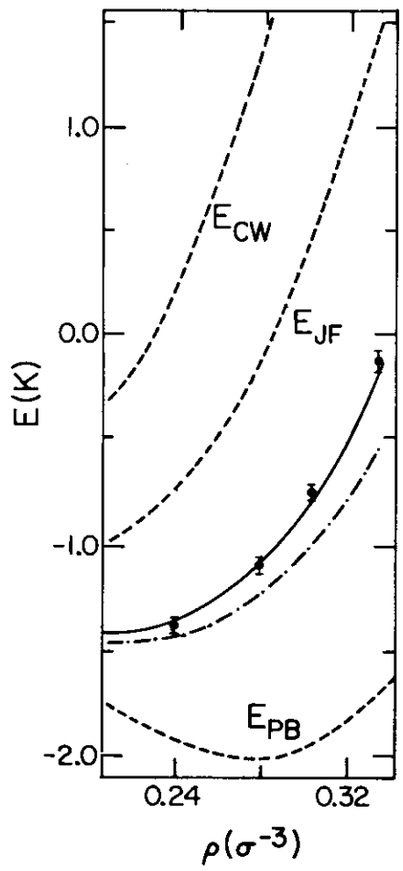

FIG. 3. Comparison of JF, PB, and CW energies in the FHNC/0 (dashed curve) and FHNC/S (solid curve) approximations with MC results using the McMillan f for normal ^{3}He. Dotted-dashed curve represents the results of FHNC/S calculations with "optimized" f_B.

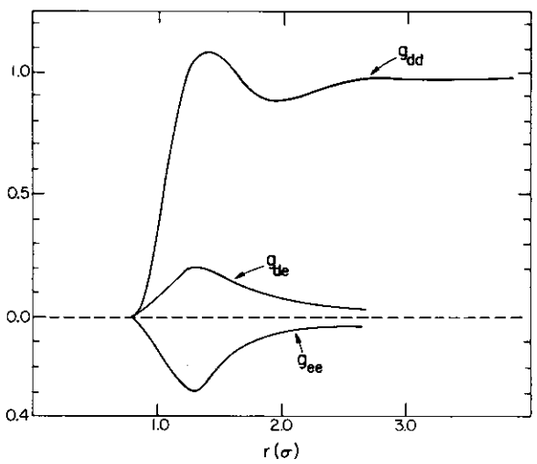

FIG. 4. Typical g_{dd}, g_{de}, and g_{ee} functions at $\rho=0.277\sigma^{-3}$ in the Jastrow approximation.

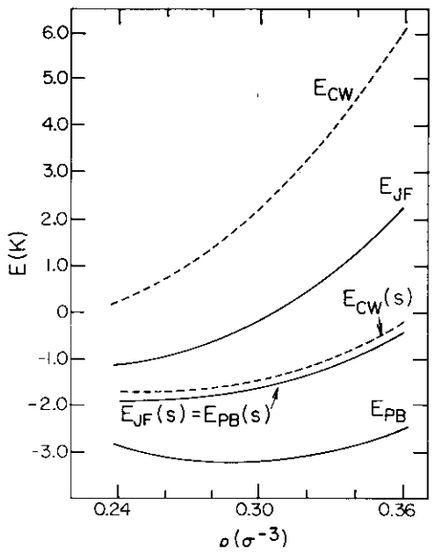

FIG. 5. Results of Jastrow calculations for fully polarized ^{3}He. Top and lower dashed curves represent the E_{CW} energies in FHNC/0 and FHNC/S approximations, respectively. Upper and lower solid curves represent the E_{JF} and E_{PB} energies in FHNC/0 approximation. Middle solid curve represents the FHNC/S energies obtained by equalizing $E_{JF}(s)$ and $E_{PB}(s)$. All calculations are carried out by using McMillan's f.

Jastrow-Slater wave function has been resolved.[19] However, we have used here a simpler method. The $f_2(r)$ in a Bose liquid is characterized by its asymptotic behavior

$$f_2(r\to\infty)=1-\alpha/r^2 . \tag{2.28}$$

The method of obtaining $f_2(r)$ with this asymptotic behavior, by minimizing the energy is given in Ref. 11. We obtain with it a family of $f_2(r,\alpha)$ by minimizing the mass-3 Bose liquid energy, and treat α as a variational parameter for the Jastrow-Slater calculation of Fermi liquid ^{3}He. The energies obtained with the $f_2(r,\alpha)$ for the normal liquid are shown in Fig. 3 by the dashed-dotted curve. They are a little below those obtained with the McMillan $f_2(r)$ of Eq. (2.27). However, in the case of spin-polarized liquid the McMillan $f_2(r)$ with $b=1.12\sigma$ gives energies a little lower than the $f_2(r,\alpha)$. We note that in Jastrow theory the normal liquid ^{3}He is very underbound and the spin-polarized liquid is energetically favored.

TABLE I. Results of FHNC/S calculations for normal ^{3}He in Jastrow approximation. The correlation function (2.17) was used with $b=1.15\sigma$. MC values E(MC) are from Ref. 1.

$\rho(\sigma^{-3})$	Scaling factor s	E (FHNC/S) $E_{PB}=E_{JF}$	E_{CW}	E (MC)
0.237	2.86	−1.37	−1.34	−1.40±0.01
0.277	3.20	−1.08	−1.07	−1.08±0.03
0.300	3.34	−0.76	−0.74	−0.70±0.05
0.330	3.60	−0.16	−0.14	−0.10±0.05

TABLE II. Results of FHNC/S calculations in Jastrow approximation for polarized ^{3}He using McMillan's f_2 with $b=1.12\sigma$.

$p\ (\sigma^{-3})$	Scaling factor s	E (FHNC/S) $E_{PB}=E_{JF}$	E_{CW}
0.237	3.80	−1.88	−1.72
0.277	3.90	−1.85	−1.68
0.300	3.96	−1.66	−1.47
0.330	4.02	−1.21	−1.00
0.360	4.10	−0.49	−0.25

III. THREE-BODY CORRELATION

In this section we use the FHNC/S method to calculate the binding energies with the wave function

$$\Psi=\prod_{\substack{i,j\\ i<j}} f_2(r_{ij}) \prod_{\substack{i,j,k\\ i<j<k}} f_3(r_{ij},r_{jk},r_{ki})\Phi . \tag{3.1}$$

Previous studies[1,4,12] have shown that the dominant three-body correlations in liquid ^{3}He are of the form

$$f_3(r_{ij},r_{jk},r_{ki})=\exp[-\tfrac{1}{2}q(r_{ij},r_{jk},r_{ki})] , \tag{3.2a}$$

$$q(r_{ij},r_{jk},r_{ki})=\sum_{\text{cyc}}\xi(r_{ij})\xi(r_{ik})(\hat{r}_{ij}\cdot\hat{r}_{ik}) , \tag{3.2b}$$

where $\sum_{\text{cyc}}$ represents a sum over the three terms obtained by replacing ijk with jki and kij, and $\hat{r}_{ij}$ and $\hat{r}_{ik}$ are unit vectors.

The FHNC equations for the distribution functions with this wave function are given in Ref. 4. They are obtained by replacing $N_{xy}+E_{xy}$ in Eqs. (2.3) and (2.4) by $N_{xy}+E_{xy}+C_{xy}$, where C_{xy} are given by

$$C_{dd}(r_{ij})=\Gamma((g_{dd}+2g_{de})_{ik},(g_{dd})_{kj}) , \tag{3.3a}$$

$$C_{de}(r_{ij})=\Gamma((g_{ee}+g_{de})_{ik},(g_{dd})_{kj})+\Gamma((g_{de})_{ik},(g_{de})_{kj}) , \tag{3.3b}$$

$$C_{ee}(r_{ij})=\Gamma((2g_{ee}+g_{de})_{ik},(g_{de})_{kj}) , \tag{3.3c}$$

$$C_{cc}(r_{ij})=\Gamma((g_{cc})_{ik},(g_{cc})_{kj}) , \tag{3.3d}$$

$$\Gamma((X)_{ik},(Y)_{kj})=\rho\int d^3r_k[f_3^2(r_{ij},r_{jk},r_{ki})-1]\times X(r_{ik})Y(r_{kj}) . \tag{3.3e}$$

The C's are new diagrammatic elements dressed with chains due to f_3. The form of Eqs. (2.7) for N_{xy} is not affected by the presence of f_3.

The three-particle distribution function is now given by

$$g_3(r_{ij},r_{jk},r_{ki})=f_3^2(r_{ij},r_{jk},r_{ki})\times\sum_{\text{exch}}g_{xy}(r_{ij})g_{y'z}(r_{jk})g_{z'x'}(r_{ki})\times[1+A_{x''y''z''}(r_{ij},r_{jk},r_{ki})] . \tag{3.4}$$

Following the method outlined in Ref. 12, we write the sum of elementary and Abe diagrams as

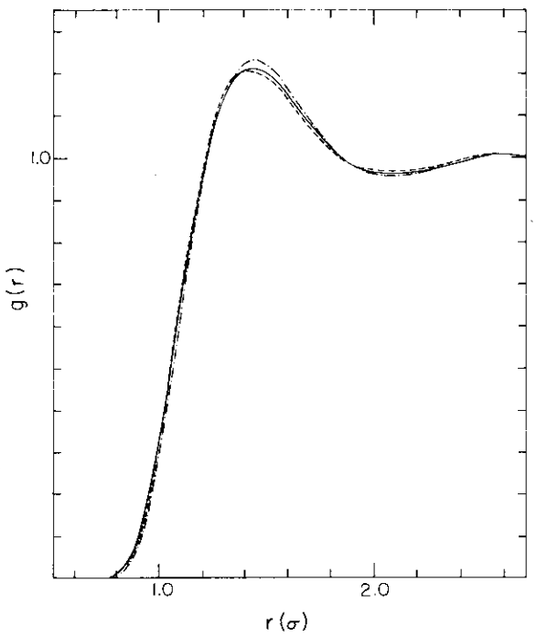

FIG. 6. Comparison of two-body distribution function $g(r)$ for different choices of the wave function. Dashed, dotted-dashed, and solid curves represent, respectively, the distribution function with Jastrow (J), Jastrow plus three-body ($J+T$), and Jastrow plus three-body plus backflow ($J+T+B$) wave functions.

$$E_{xy}=E^g_{xy}+E^t_{xy} \ , \tag{3.5}$$

$$A_{xyz}=A^g_{xyz}+A^t_{xyz} \ , \tag{3.6}$$

where E^g and A^g are sums of diagrams having only $g_{x'y'}$ correlations, while E^t and A^t must have one or more explicit three-body correlations. The pair distribution $g(r)$ (Fig. 6) does not change significantly by the inclusion of f_3. Thus the approximations (2.24) and (2.25), with scaling factor s determined from the Jastrow-Slater calculation, are used for E^g and A^g. E^t_{dd} and A^t_{ddd} are approximated by the sum of four-point diagrams[12] $E^t_{dd,4}$ and $A^t_{ddd,4}$, and the E^t_{xy} $(x,y\neq d,d)$, A^t_{xyz} $(x,y,z\neq d,d,d)$ are neglected. The distribution function $g(r)$ given by Eq. (2.2) is used in the calculation of E^t and A^t so that four-point diagrams with one g_{xy} $(xy\neq dd)$ are counted correctly.

The PB and CW energies with wave function (3.1) depend upon four- and five-particle distribution functions. Hence only the $E_{\rm JF}$ is calculated,

$$E_{\rm JF}=T_F+W_B+W_\phi+U_\phi+U_T \ , \tag{3.7}$$

where U_T is the kinetic energy due to f_3,

$$U_T=\frac{\hbar^2\rho^2}{16m}\int d^3r_{ij}d^3r_{ik}g_3(r_{ij},r_{jk},r_{ki})\nabla_i^2 q(r_{ij},r_{jk},r_{ki}) \ . \tag{3.8}$$

The T_F and W_B are given by Eqs. (2.13) and (2.21), but there are minor changes in the equation for W_ϕ and U_ϕ.

TABLE III. Comparison of MC and FHNC/S energies in $J+T$ approximation.

ρ (σ^{-3})	MC f_{ijk} E (FHNC/S)	MC f_{ijk} E (MC)	Present f_{ijk} E (FHNC/S)
0.237	−1.67	−1.68±0.02	−1.73
0.277	−1.49	−1.61±0.03	−1.70
0.300	−1.14	−1.34±0.04	−1.53

The E_{cc} in Eq. (2.22) for W_ϕ must be replaced with $E_{cc}+C_{cc}$ and a factor $f_3^2(r_{ij},r_{jk},r_{ki})$ should be inserted in the U_ϕ integral [Eq. (2.23)].

In order to compare our results with the variational MC results we have calculated the $E(\rho)$ with the wave function of Ref. 1. Here the two-body correlation has the McMillan form given by Eq. (2.27), and

$$\xi(r)=\begin{cases}\sqrt{\lambda_t}r\exp\left[-\left[\dfrac{r-r_t}{\omega_t}\right]^2\right]\left[\dfrac{r-r_B}{r_B}\right]^3 & \text{for } r\le r_B \\ 0 \text{ for } > r_B \ .\end{cases} \tag{3.9}$$

The values of parameters b, λ_t, r_t, ω_t, and r_B are taken from Ref. 1. Results of our FHNC/S calculations for $E(\rho)$ are compared with the MC results in Table III. The agreement is reasonable but not as good as in the Jastrow-Slater case. It appears that the neglected E^t_{xyz} and A^t_{xyz} diagrams may have contributions of $\sim$0.1 to 0.2 K with the $\xi(r)$ of Ref. 1.

The last column of Table III gives the energies obtained after removing the box factor from the $\xi(r)$ function (i.e., $r_B\to\infty$),

$$\xi(r)=\sqrt{\lambda_t}r\exp\left[-\left[\frac{r-r_t}{\omega_t}\right]^2\right] \ . \tag{3.10}$$

The optimum values of λ_t, r_t, and ω_t were varied to minimize the FHNC/S energy at $\rho=0.277\sigma^{-3}$ and found to be

$$\lambda_t=-0.75 \ , \tag{3.11a}$$

$$\omega_t=0.45\sigma \ , \tag{3.11b}$$

$$r_t=0.85\sigma \ . \tag{3.11c}$$

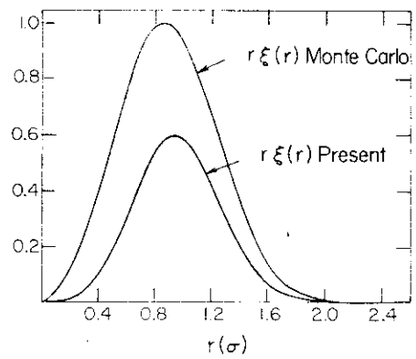

FIG. 7. Comparison of the present and MC $\xi(r)$.

TABLE IV. Calculated energies of normal ^{3}He in K; $\langle T \rangle$ and $\langle V \rangle$ denote the expectation values of kinetic and potential energies. The symbols J, $J+T$, and $J+T+B$ represent the results of calculation with wave functions (2.1), (3.3), and (4.2), respectively. All the calculations have been performed with the "optimized" correlation function f_B.

ρ (σ^{-3})	Ψ	s	$\langle T \rangle$	$\langle V \rangle$	E (var)
0.237	J		10.71	−12.17	−1.46
	$J+T$	3.14	10.40	−12.19	−1.79
	$J+T+B$		9.89	−12.11	−2.22
0.277	J		13.48	−14.76	−1.28
	$J+T$	3.52	12.97	−14.80	−1.83
	$J+T+B$		12.28	−14.64	−2.36
0.300	J		15.22	−16.28	−1.06
	$J+T$	3.82	14.55	−16.33	−1.78
	$J+T+B$		13.77	−16.12	−2.35
0.330	J		17.69	−18.29	−0.60
	$J+T$	4.13	16.76	−18.31	−1.55
	$J+T+B$		15.86	−18.03	−2.17
0.360	J		20.41	−20.28	0.126
	$J+T$	4.22	19.21	−20.25	−1.04
	$J+T+B$		18.16	−19.86	−1.70
0.384	J		22.69	−21.99	+0.70
	$J+T$	4.59	21.21	−21.91	−0.70
	$J+T+B$		20.09	−21.43	−1.34

The dependence of these variational parameters on the density is found to be negligible within the accuracy of the present work. The energies obtained with this $\xi(r)$ are much lower than those with the $\xi(r)$ of Ref. 1. The two $\xi(r)$ are plotted in Fig. 7; the $\xi(r)$ of Ref. 1 appears to be too large at small r. The present $f_3(r_{ij},r_{jk},r_{ki})$ is much weaker and hence the approximations of A^t and E^t should be less critical for the present calculations than for calculations with $\xi(r)$ of Ref. 1.

The results of calculations using the semioptimized $f_2(r_{ij})$ are given in Table IV. The optimum values of λ_t, ω_t, and r_t do not change significantly when the McMillan $f_2(r_{ij})$ is replaced by the semioptimized $f_2(r_{ij})$. [The results obtained for the spin-polarized liquid with the

TABLE V. Calculated energies for polarized ^{3}He in K. All the symbols have same meaning as in Table IV. McMillan form (2.17) was employed for the Jastrow correlation function with $b=1.12\sigma$.

ρ (σ^{-3})	Ψ	s	$\langle T \rangle$	$\langle V \rangle$	E (var)
0.237	J	3.80	10.06	−11.94	−1.88
	$J+T$		10.01	−12.02	−2.01
	$J+T+B$		9.86	−11.91	−2.05
0.277	J		12.40	−14.25	−1.85
	$J+T$	3.90	12.43	−14.49	−2.06
	$J+T+B$		12.24	−14.33	−2.09
0.300	J		14.06	−15.72	−1.66
	$J+T$	4.00	13.91	−15.85	−1.94
	$J+T+B$		13.69	−15.65	−1.96
0.330	J		16.15	−17.36	−1.21
	$J+T$	4.02	15.91	−17.51	−1.60
	$J+T+B$		15.62	−17.26	−1.64
0.360	J		18.39	−18.88	−0.486
	$J+T$	4.10	17.96	−19.03	−1.07
	$J+T+B$		17.62	−18.73	−1.11

McMillan $f_2(r)$ are given in Table V and displayed in Fig. 11.] The optimum values of the triplet parameters were found to be

$$\lambda_t=-0.6\,, \tag{3.12a}$$

$$\omega_t=0.45\sigma\,, \tag{3.12b}$$

$$r_t=0.85\sigma\,. \tag{3.12c}$$

The three-body correlations have a larger effect on the energy of the normal liquid, but in a Jastrow-plus-triplet theory the spin-polarized liquid has lower energy as was noted earlier.[3]

IV. BACKFLOW CORRELATIONS

Momentum-dependent two-body correlations, called backflow correlations, were introduced in the variational wave function of liquid ^{3}He in Ref. 4 to generate the Feynman-Cohen[20] backflow. Following Ref. 1 we take it of the form

$$f_k(i,j)=\exp\{i\eta(r_{ij})\vec{r}_{ij}\cdot[\vec{K}(i)-\vec{K}(j)]\}\,, \tag{4.1}$$

which is identical to that in Ref. 4,

$$f_k(i,j)\simeq 1+i\eta(r_{ij})\vec{r}_{ij}\cdot[\vec{K}(i)-\vec{K}(j)]\,, \tag{4.2}$$

when $\eta(r)\ll 1$. $\vec{K}(i)$ are operators that operate on the Φ in the manner prescribed below.

The variational wave function is

$$\Psi=\left[\prod_{\substack{i,j\\ i<j}} f_2(r_{ij})\right]\left[\prod_{\substack{i,j,k\\ i<j<k}} f_3(r_{ij},r_{jk},r_{ki})\right]\left[\prod_{\substack{i,j\\ i<j}} f_k(ij)\right]\Phi\,, \tag{4.3}$$

and the antisymmetrized Fermi gas Φ contains a sum of terms

$$\Phi=\sum_{\text{perm}}(-1)^P\exp\left[i\sum_i \vec{k}_{n(i)}\cdot\vec{r}_i\right]\,, \tag{4.4}$$

where $\vec{k}_{n(i)}$ is the momentum state occupied by particle i and P is the number of pair exchanges required to reach the state characterized by $n(i)$, from the simple product state Φ_Π having $n(i)=i$,

$$\Phi_\Pi=\exp\left[i\sum_i \vec{k}_i\cdot\vec{r}_i\right]\,. \tag{4.5}$$

The "operators" $K(i)$ operate on the Φ as

$$\vec{K}(i)\exp\left[i\sum_i \vec{k}_{n(i)}\cdot\vec{r}_i\right)=\vec{k}_{n(i)}\exp\left[i\sum_i \vec{k}_{n(i)}\cdot\vec{r}_i\right]\,. \tag{4.6}$$

The $\vec{K}(i)$ in Ψ^* must operate on the Φ^*. Thus the variational wave function of Eq. (4.3) is interpreted as

$$\Psi=\left[\prod_{\substack{i,j\\ i<j}} f(r_{ij})\right]\left[\prod_{\substack{i,j,k\\ i<j<k}} f_3(r_{ij},r_{jk},r_{ki})\right]\left[\sum_{\text{perm}}\left[\prod_{\substack{i,j\\ i<j}}\exp[i\eta(r_{ij})\vec{r}_{ij}\cdot(\vec{k}_{n(i)}-\vec{k}_{n(j)}]\right](-1)^P\exp\left[i\sum_i \vec{k}_{n(i)}\cdot\vec{r}_i\right]\right]\,. \tag{4.7}$$

Expectation values with this wave function can be more conveniently calculated by antisymmetrizing only the left-hand side,

$$\frac{\langle\Psi|O|\Psi\rangle}{\langle\Psi|\Psi\rangle}=\frac{\int\Phi^*\left[\prod f_k^{*L}\right]\left[\prod f_3\right]\left[\prod f_2\right]O\left[\prod f_2\right]\left[\prod f_3\right]\left[\prod f_k^{R}\right]\Phi_\Pi d\tau}{\int\Phi^*\left[\prod f_k^{L}\right]\left[\prod f_3^2\right]\left[\prod f_2^2\right]\left[\prod f_k^{R}\right]\Phi_\Pi d\tau}\,, \tag{4.8}$$

where f_k^L operates to the left and f_k^R to the right. Diagrammatic cluster expansions are obtained by expanding the many-body integrals in terms of the quantities $f_2^2(r_{ij})-1$, $f_3^2(r_{ij},r_{jk},r_{ki})-1$, and $f_k(i,j)-1$, and canceling the disconnected and reducible pieces of the numerator against the denominator. The cancellation of the reducible diagrams may not be exact for wave functions containing backflow correlations, as discussed in Ref. 4.

It is difficult to sum chains of backflow correlations. In Ref. 4 the effect of backflow correlations on only dressed two- and three-body clusters was considered. Comparisons with MC calculations suggest that it is not a bad approximation, and hence we continue to use it in the present work. The formulation of Ref. 4 needs to be modified to use f_k of the form (4.1). This form of f_k has great advantages in MC calculations.

We first consider the effect of f_k on the distribution functions. The large direct diagrams, which come from the term in Φ^* and have $n(i)=i$, are not affected by f_k. In these diagrams

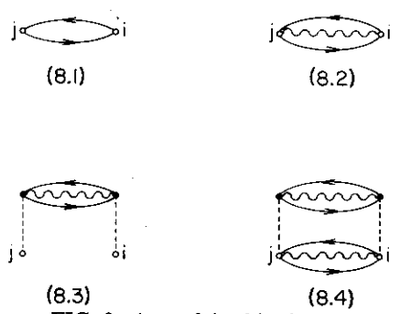

FIG. 8. As explained in the text.

$$f_k^{*L}(i,j)=\exp[-i\eta(r_{ij})\vec{r}_{ij}\cdot(\vec{k}_i-\vec{k}_j)]=1/f_k^R(i,j)\ , \tag{4.9}$$

and thus

$$\left[\prod f_k^{*L}(i,j)\right]\left[\prod f_k^R(i,j)\right]=1 \tag{4.10}$$

in direct diagrams. This fact, together with small magnitude and range of $\eta(r)$ probably make the present treatment of the effect of f_k on the distribution functions and energy adequate.

In Jastrow theory the two-body exchange diagram (8.1) of Fig. 8 gives the following contribution to g_{ee}:

$$\sum_{k,\sigma} g_{dd}(r_{ij})\exp(i\vec{k}_i\cdot\vec{r}_{ij})\exp(i\vec{k}_j\cdot\vec{r}_{ji})\ , \tag{4.11}$$

which upon summing over spins and momentum states,

$$\frac{\nu}{N}\sum_{k\le k_f} e^{i\vec{k}\cdot\vec{r}}=l(k_Fr)\ , \tag{4.12}$$

becomes $-g_{dd}(r)l^2(k_Fr)/\nu$. This exchange contribution comes from the term in Φ^* in which $n(j)=i$, $n(i)=j$, and the other $n(k)=k$. We now want to add the contribution of the diagram (8.2), in which the wavy line represents $(f_k^{*L}f_k^R-1)$, to (8.1). When i and j are exchanged we have

$$f_k^{*L}(i,j)f_k^R(i,j)=\exp[2i\eta(r_{ij})\vec{r}_{ij}\cdot(\vec{k}_i-\vec{k}_j)]\ . \tag{4.13}$$

Thus the sum of (8.1) and (8.2) is obtained as

$$\begin{aligned}&-\sum_{k,\sigma} g_{dd}(r_{ij})\exp\{i\vec{k}_i\cdot\vec{r}_{ij}[1+2\eta(r_{ij})]+i\vec{k}_j\cdot\vec{r}_{ji}[1+2\eta(r_{ij})]\}\\&\quad=-g_{dd}(r_{ij})l^2(k_Ft(r_{ij}))/\nu\ ,\\&t(r)=r[1+2\eta(r)]\ .\end{aligned} \tag{4.14}$$

The $l(k_Fr_{ij})$ in the FHNC/S equation (2.4) is replaced by $l(k_Ft(r_{ij}))$. In this way the contribution of many diagrams having f_k correlations, of the type illustrated in Fig. 8, are correctly summed.

Some of the diagrams in which three particles are involved in exchange with f_k correlations are shown in Fig. 9. These diagrams have rather small contributions which are calculated approximately with expansion (4.2). The $f_k^{*L}f_k^R-1$ in diagram (9.1) is $i\eta(r_{ik})\vec{r}_{ik}\cdot(\vec{k}_i-\vec{k}_j)$, up to order $\eta(r)$. Thus the contribution of (9.1) is given by

$$-2\rho g_{dd}(r_{ij})l(k_Fr_{ij})l'(k_Fr_{ij})\int\cos\theta_i r_{ik}\eta(r_{ik})g_{dd}(r_{ik})(g_{dd}(r_{jk})-1)f_3^2d^3r_k=-g_{dd}(r_{ij})\left[\frac{\partial}{\partial r}l^2(k_Fr_{ij})\right]Z_0(r_{ij})\ , \tag{4.15}$$

$$Z_0(r_{ij})=\rho\int\cos\theta_i r_{ik}\eta(r_{ik})g_{dd}(r_{ik})[g_{dd}(r_{jk})-1]f_3^2d^3r_k\ . \tag{4.16}$$

Diagrams with f_k correlations between jk double this contribution. We can include it in the contribution of diagram (8.1) by replacing $l(k_Fr)$ with $l(k_Fr)(1+2Z_0(r))$. We also include the contributions of diagrams (8.2) and (9.2) and many others by replacing $l(k_Fr_{ij})$ by $l(k_Ft_{ij})$ in Eq. (2.4) with

$$t=r[1+2\eta(r)+2Z(r)]\ , \tag{4.17}$$

where

$$\begin{aligned}Z(r)=\rho\int&\cos\theta_i r_{ik}\eta(r_{ik})\\&\times\{g_{dd}(r_{ik})[g_{dd}(r_{jk})+g_{de}(r_{jk})]\\&+g_{de}(r_{ik})g_{dd}(r_{jk})\}f_3^2d^3r_k\ .\end{aligned} \tag{4.18}$$

The terms involving the product $g_{dd}g_{de}$ in the above equation can be understood following the discussion of diagrams (9.5) and (9.6) given later on.

Contributions of diagrams (9.3)–(9.9) cannot be summed by modifying the Slater function $l(x)$. They give new FHNC elements[4] denoted by D_{xy}, which must be added to the three-body elements C_{xy}. Diagrams (9.3) and (9.4) contribute to D_{ed} as follows:

$$\begin{aligned}D_{ed}(ij)=&2\rho r_{ij}\eta(r_{ij})\\&\times\int d^3r_k l_p(r_{ik})g_{cc}(r_{ik})\cos\theta_i g_{dd}(r_{jk})f_3^2\\&+2\rho\int d^3r_k l_p(r_{ik})g_{cc}(r_{ik})\\&\times\cos\theta_k r_{jk}\eta(r_{jk})g_{dd}(r_{jk})f_3^2\ ,\end{aligned} \tag{4.19}$$

where

$$l_p(r)\equiv\frac{\partial l(k_Ft(r))}{\partial t(r)}\ . \tag{4.20}$$

Two types of diagrams contribute to $D_{ee}(ij)$,

$$D_{ee}(ij)=D_{ee}(ij)_1+D_{ee}(ij)_2\ . \tag{4.21}$$

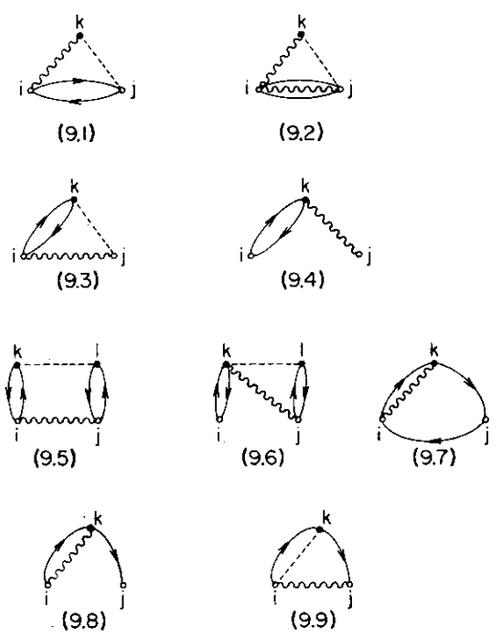

FIG. 9. As explained in the text.

The $D_{ee}(ij)_1$ is twice the contribution obtained by replacing $g_{dd}(r_{jk})$ by $g_{de}(r_{kj})$ in $D_{ed}(ij)$. It sums diagrams of type (9.5) and (9.6). The $(f_k^{*L}f_k^R-1)$ in diagram (9.6) is given by

$$i\eta(r_{jk})\vec{r}_{jk}\cdot[(\vec{k}_k-\vec{k}_i)-(\vec{k}_j-\vec{k}_l)]+\cdots , \tag{4.22}$$

where the ellipsis represents terms in η^2 and higher, and the $\vec{r}_{jk}\cdot(\vec{k}_k-\vec{k}_i)$ part of it contributes to the D_{ee}. The $\vec{r}_{jk}\cdot(\vec{k}_j-\vec{k}_l)$ part has cos of the angle j of triangle kjl, and its contribution is contained in the chain formed by the $D_{de}(k,j)$ cluster, containing jkl and the ee link ki. The $D_{ee}(i,j)_2$ is given by

$$D_{ee}(i,j)_2=4\rho l_p(r_{ij})\int d^3r_k\cos\theta_i r_{ik}\eta(r_{ik}) \times g_{cc}(r_{ik})g_{cc}(r_{kj})f_3^2 . \tag{4.23}$$

The wavy line in these diagrams is

$$i\eta(r_{ij})\vec{r}_{ik}\cdot(2\vec{k}_i-\vec{k}_k-\vec{k}_j) , \tag{4.24}$$

the $\vec{r}_{ik}\cdot\vec{k}_i$ part is summed by the substitution $l(k_Fr)\to l(k_Ft)$, the $\vec{r}_{ik}\cdot\vec{k}_j$ part gives the contribution (4.23), and the $\vec{r}_{ik}\cdot\vec{k}_k$ term is included in D_{cc}. The factor 4 in (4.23) comes from summing over the diagrams having ik and jk wavy lines, and exchanges in both directions.

The three-body elements (9.8) and 9.9) contribute to D_{cc}. The correlation in (9.8) is given by (4.24) and the relevant term is $\vec{r}_{ik}\cdot\vec{k}_j$, while that in (9.9) is given by

$$i\eta(r_{ij})\vec{r}_{ij}\cdot(\vec{k}_i-\vec{k}_j-\vec{k}_l+\vec{k}_k) , \tag{4.25}$$

where we assume that particle i goes in state l. The D_{cc} includes contributions from the $\vec{r}_{ij}\cdot(\vec{k}_j+\vec{k}_k)$ term. We obtain

$$D_{cc}(i,j)=\frac{-2}{\nu}\rho\int d^3r_k g_{cc}(r_{ik})r_{ik}\eta(r_{ik})\cos\theta_k l_p(r_{kj})[g_{dd}(r_{kj})-1] + \frac{-2}{\nu}\rho\int d^3r_k[g_{dd}(r_{ik})-1](l_p(r_{ik})\cos\theta_i r_{ij}\eta(r_{ij})g_{cc}(r_{jk})f_3^2 , \tag{4.26}$$

after subtracting the contribution of separable diagrams.[4] These D_{xy} sum all dressed three-body elements linear in η. Contributions of order η^2 (or higher) to three-body elements are not summed exactly in the present work. The contributions to clusters having four or more particles connected by exchanges for f_k correlations are also not exactly treated.

The JF energy is given by

$$E_{\rm JF}=T_F+W_B+W_\phi+U_\phi+U_T+T_B+T_k , \tag{4.27}$$

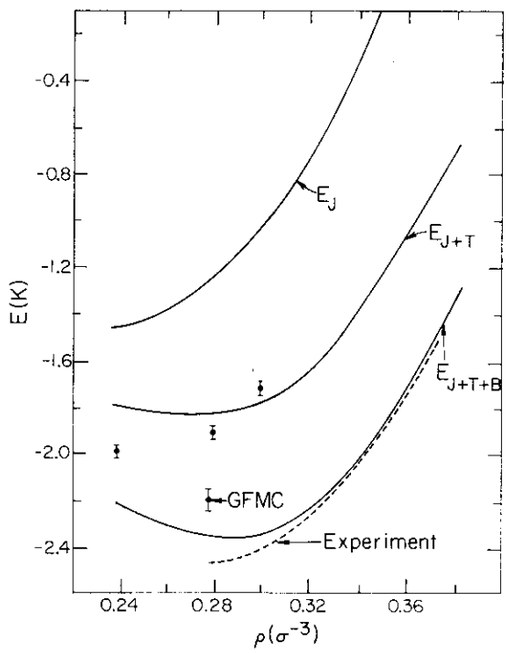

FIG. 10. Comparison of the calculated energies for normal ^{3}He with experiment (Refs. 21 and 22), Green's-function MC (Ref. 5), and variational MC (Ref. 1) (unlabeled points with error bars) calculations. Symbols J, $J+T$, and $J+T+B$ are explained in Fig. 6.

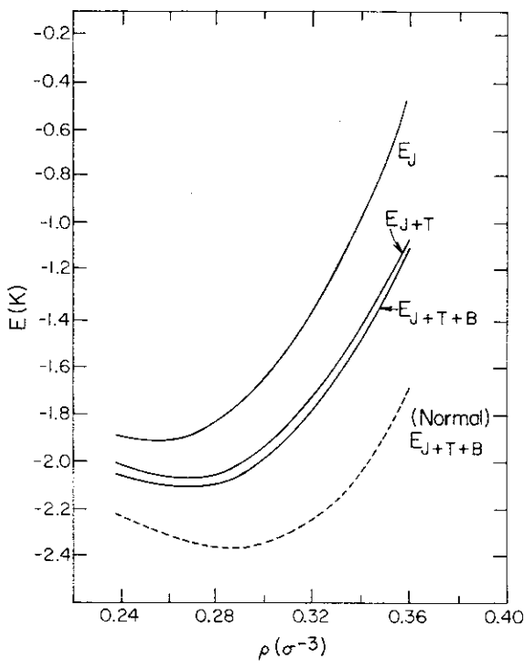

FIG. 11. Calculated polarized ^{3}He energies. Dashed curve representing the normal ^{3}He energies is drawn for comparison purposes.

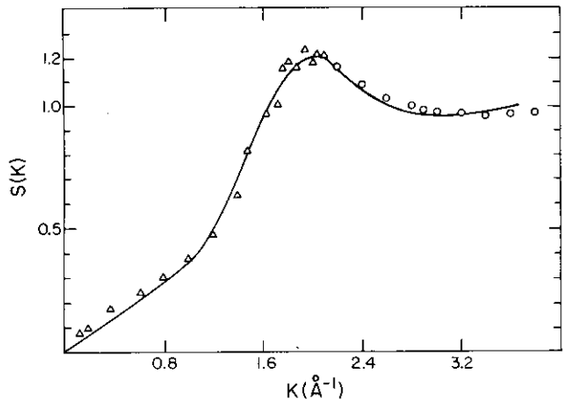

FIG. 12. Calculated liquid structure function $S(k)$ (solid curve) compared with experiment. Triangles represent the data from Ref. 23 at $T=0.41$ K and circles represent the data from Ref. 24 at $T=0.76$ K.

and the terms T_F to U_T are discussed earlier. W_ϕ is given by

$$W_\phi=-\frac{\hbar^2}{4m}\frac{\rho}{\nu}\times\int d^3r\{g_{dd}[l-\nu(N_{cc}+E_{cc}+C_{cc}+D_{cc})\times\nabla_i^2 l(k_F t)+l_p^2]+\nu N_{cc}\nabla^2 l\}\ . \tag{4.28}$$

There are minor modifications in U_ϕ of Eq. (2.23): (i) we replace l by l_p, and (ii) insert f_3^2 in the integral. The expressions for T_F [Eq. (2.13)], W_B [Eq. (2.21)], and U_T [Eq. (3.8)] are unchanged; these quantities change only via the changes in the distribution functions.

The T_B represents the JF kinetic energy of the backflow correlation. Let B denote the product of pair and triplet correlations in the Ψ [Eq. (4.3)], let F denote the product of f_k^R, and let $F^\dagger$ denote the product of f_k^{*L}. We then have

$$T_B=-\frac{\hbar^2}{8m}\{\langle\Phi^*(\nabla_1^2F^\dagger)B\,|\,\psi\rangle+\langle\Psi\,|\,B(\nabla_1^2F)\Phi\rangle-2\langle\Phi^*(\vec\nabla_1F^\dagger)B\,|\,B(\vec\nabla_1F)\Phi\rangle\}/\langle\Psi\,|\,\Psi\rangle\ . \tag{4.29}$$

The T_K term comes from $F^\dagger\neq F$,

$$T_K=\frac{\hbar^2}{2m}\frac{\langle\Psi\,|\,B(\vec\nabla_1F)\cdot\vec\nabla_1\Phi\rangle-\langle(\vec\nabla_1\Phi^*)F^\dagger B\,|\,B(\vec\nabla_1F)\Phi\rangle}{\langle\Psi\,|\,\Psi\rangle}\ . \tag{4.30}$$

In Ref. 4 the dressed-cluster expansion is used to calculate terms analogous to T_B and T_k in the PB energy expression. It was found that reasonable results are obtained by retaining only the two-body terms. Hence we calculate T_k in that approximation as follows:

$$T_B\approx\frac{\hbar^2k_F^2}{5m}\rho\int d^3r(\eta'^2r^2+2\eta\eta'r+3\eta^2)[g_{dd}(r)+g_{de}(r)]-\frac{\hbar^2}{2m}\rho\int d^3r(\eta''r+4\eta')g_{cc}(r)l_p(r)\ , \tag{4.31}$$

$$T_K\approx\frac{\hbar^2k_F^2}{5m}\rho\int d^3r(\eta'r+3\eta)[g_{dd}(r)+g_{de}(r)]\ . \tag{4.32}$$

The $\eta(r)$ is parametrized as in Ref. 1, except for the box term (necessary in MC calculations) which is removed,

$$\eta(r)=\lambda_\eta\exp\left[-\left[\frac{r-r_\eta}{\omega_\eta}\right]^2\right]\ . \tag{4.33}$$

The optimum values obtained at $\rho=0.277\sigma^{-3}$ for the normal (polarized) ^{3}He liquid are the following:

$$\lambda_\eta=0.2(0.05)\ ,\quad r_\eta=0.8(0.8)\ ,\quad \omega_\eta=0.375(0.375)\ . \tag{4.34}$$

These values are used at all densities, and the calculated energies are shown in Tables IV and V and Figs. 10 and

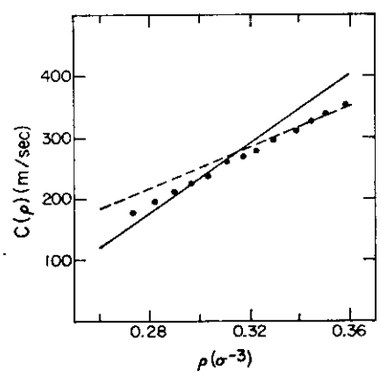

FIG. 13. Sound velocities $C(\rho)$ in m/sec for normal ^{3}He (solid curve) and polarized ^{3}He (dashed curve). Dots represent the experimental data from Ref. 21.

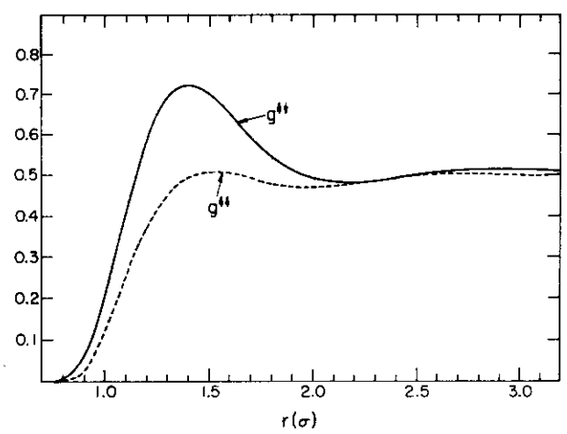

FIG. 14. Distribution function of normal ^{3}He for parallel spins $g_{\uparrow\uparrow}$ and antiparallel $g_{\uparrow\downarrow}$ at $\rho=0.277\sigma^{-3}$.

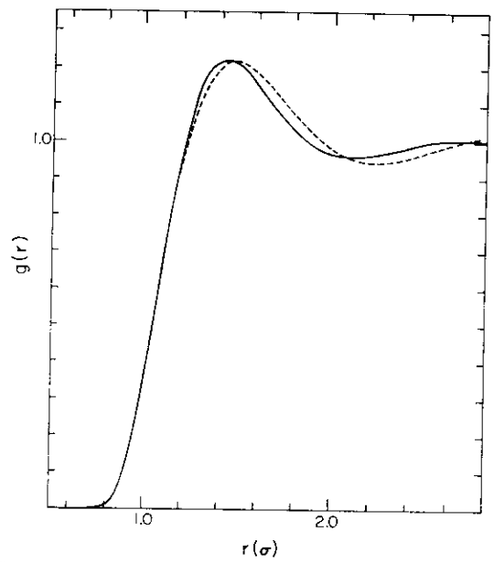

FIG. 15. Comparison of the two-body distribution functions for the normal (solid curve) and polarized (dashed curve) ^{3}He at $\rho=0.277\sigma^{-3}$.

11. The calculated $E(\rho)$ of the normal liquid is in fair agreement with the experiment, and a little below the GFMC upperbound.[5] The uncertainties in the present calculation are of the order of 0.1 K, and so the differences between the present results and either the GFMC or experimental results cannot be meaningfully analyzed. A MC calculation with the present wave function would be instructive. The liquid structure factor (Fig. 12), and the sound velocity (Fig. 13) are in good agreement with experimental data. Best of all, the normal liquid has lower energy than the spin-polarized liquid. The backflow correlation has very little effect on the $E(\rho)$ of the polarized liquid and thus makes the normal phase stable. This correlation is meant to represent the k (relative momentum) and l (angular momentum) dependence of the pair correlation. The $f_2(k,l)$ was studied in a crude approximation by Pandharipande and Bethe,[25] who find that the k and l dependence is strongest for $l=0$. The $l=0$ correlations are much different from the average correlation in $l\neq 0$ states, and also have significant k dependence. The polarized liquid has no $l=0$ pairs due to antisymmetry, and thus it is not surprising that the backflow correlations have little effect on this phase. The calculated pair-distribution functions are given in Figs. 14 and 15; the difference between $g_{\uparrow\uparrow}$ and $g_{\uparrow\downarrow}$ in normal liquid is substantial, but that between the total g in normal and polarized liquids is relatively smaller.

ACKNOWLEDGMENTS

This work was supported by the U.S. Department of Energy, Division of Materials Sciences, under Grant No. DE-AC02-76ER01198, and North Atlantic Treaty Organization (NATO) Travel Grant No. 0453/82.

*On leave from the University of Pisa, Pisa, Italy.
†On leave from Department of Physics, Aligarh Muslim University, Aligarh, India.

[1]K. E. Schmidt, M. A. Lee, M. H. Kalos, and G. V. Chester, Phys. Rev. Lett. 47, 807 (1981).
[2]D. Levesque, Phys. Rev. B 21, 5159 (1980).
[3]C. Lhuillier and D. Levesque, Phys. Rev. B 23, 2203 (1981).
[4]K. E. Schmidt and V. R. Pandharipande, Phys. Rev. B 19, 2504 (1979).
[5]M. A. Lee, K. E. Schmidt, M. H. Kalos, and G. V. Chester, Phys. Rev. Lett. 46, 728 (1981).
[6]P. A. Whitlock, D. M. Ceperley, G. V. Chester, and M. H. Kalos, Phys. Rev. B 19, 5598 (1979).
[7]M. H. Kalos, M. A. Lee, P. A. Whitlock, and G. V. Chester, Phys. Rev. B 24, 115 (1981).
[8]R. A. Aziz, V. P. S. Nain, J. S. Carley, W. L. Taylor, and G. T. McConville, J. Chem. Phys. 70, 4330 (1979).
[9]E. Krotschek, R. A. Smith, J. W. Clark, and R. M. Panoff, Phys. Rev. B 24, 6383 (1981).
[10]J. C. Owen and G. Ripka, Phys. Rev. B 25, 4914 (1982).
[11]Q. N. Usmani, B. Friedman, and V. R. Pandharipande, Phys. Rev. B 25, 4502, (1982).
[12]Q. N. Usmani, S. Fantoni, and V. R. Pandharipande, Phys. Rev. B 26, 6123 (1982).
[13]K. Schmidt, M. H. Kalos, and Michael A. Lee, Phys. Rev. Lett. 45, 573 (1980).
[14]V. R. Pandharipande, J. G. Zabolitzky, Steven C. Piper, R. B. Wiringa, and U. Helmbrecht, Phys. Rev. Lett. 50, 1676 (1983).
[15]S. Fantoni and S. Rosati, Lett. Nuovo Cimento 10, 545 (1974); Nuovo Cimento A 25, 593 (1975).
[16]J. G. Zabolitzky, Adv. Nucl. Phys. 12, 1 (1981).
[17]R. Abe. Prog. Theor. Phys. 21, 421 (1959).
[18]H. J. Jackson and E. Feenberg, Ann. Phys. (N.Y.) 15, 266 (1961).
[19]L. J. Lantto and P. J. Siemens, Phys. Lett. 68B, 308 (1977).
[20]R. P. Feynman and Michael Cohen, Phys. Rev. 105, 1189 (1956).
[21]Barnard M. Abraham and Darrell W. Osborne, J. Low Temp. Phys. 5, 335 (1971).
[22]T. R. Roberts, R. H. Sherman, and S. G. Sydoriak, J. Res. Natl. Bur. Stand. 68A, 567 (1964).
[23]R. B. Hallock, Phys. Rev. A 5, 320 (1972).
[24]E. K. Achter and L. Meyer, Phys. Rev. 188, 51 (1969).
[25]V. R. Pandharipande and H. A. Bethe, Phys. Rev. C 7, 1312 (1973).